

Working Principle and Experimental Results for a Differential Phase-Doppler Technique

Jörg Rheims*, Thomas Wriedt**, Klaus Bauckhage*

Dedicated to Professor Dr. Heinz Fissan on the occasion of his 60th birthday

(Received: 25 March 1998; resubmitted: 26 June 1998)

Abstract

By replacing the two detectors of a standard phase-Doppler anemometer (PDA) with a charge coupled device (CCD) line scan sensor, the scattered light can be measured not only with high temporal but also with improved spatial resolution. Thereby, the quantity to be measured by PDA, the phase difference $\Delta\phi$, can be determined as function of the elevation angle ψ . This allows a statistical evaluation of the received signal and permits precise measurements of the size and velocity even of non-ideal solid

particles with inhomogeneous composition, aspherical shape or rough surface.

In this paper, the basis of data acquisition and evaluation is described. This is followed by experimental results for glass spheres with intact and defect surfaces and, for comparison, for water droplets. These results demonstrate the potential of this measuring device, described as a differential phase-Doppler anemometer (DPDA).

1 Introduction

Phase-Doppler anemometry (PDA) is a versatile tool for in situ measurements of the size and velocity of dispersed spherical particles in various types of two-phase flows. It is, however, mainly limited to homogeneous particles with smooth surfaces. If the investigated particles do not meet these requirements, as most solid particles do, the scattered light bears irregular and ambiguous information about the phase difference $\Delta\phi$, which leads to incorrect particle size measurements. This restriction has been with PDA from its very beginnings [1].

Especially the size of solid particles is extremely difficult to measure: as a result of their formation process, their shape is not always perfectly spherical and their surface might be covered with small distortions such as cavities, satellite particles or oxide layers. If transparent particles such as glass beads are investigated, their inner structure plays an additional role in the scattering process; within the particle there may exist different types of inclusions (gas bubbles, minerals, etc.) or microcracks [2].

To overcome this deficiency, different strategies have been developed; for instance, the experimental set-up and the signal processing scheme have been modified. Dual-mode PDA [3] combines a planar PDA with a standard PDA so that two phase differences are measured per scattering event. The two phase difference data points are validated against each other to decide whether the signal is accepted for evaluation or discarded. This permits the detection of scattering events which are distorted, for example, by multiple scattering in dense flows, poor surface quality, etc. Dual-mode PDA permits measurements under such

severe conditions, but at the possible expense of a reduced acceptance rate.

Another approach is based on a mathematical correction of measured polydisperse size distributions by a deconvolution technique [4]. This method was later verified experimentally [5] by investigating suspension droplets. The deconvolution method showed its aptitude for size measurements of such inhomogeneous fluids, but it has the disadvantage that the correlation between the distributions of particle size and velocity is lost. Furthermore, deconvolution requires at least 5000 data points.

In this paper, a method is described in which the two detectors of a standard PDA system are replaced by a charge coupled device (CCD) line scan sensor with 256 pixels. Hence the light scattered by the particle can be measured with high spatial resolution. Instead of two signals, 256 signals are detected, which leads to 128 phase difference values instead of only one. By statistically evaluating the scattered signal, even severely distorted signals can be analyzed and need not be discarded. Furthermore, the correlation between the measured size and velocity information is conserved. For this device we suggest the term ‘‘differential phase-Doppler anemometry’’ (DPDA).

The experimental set-up of DPDA will be described in the next section, followed by the description of an optimization procedure based on light scattering computations. In the fourth section, the technique of signal evaluation will be described. Finally, selected experimental results will be given. These results demonstrate that several of the restrictions imposed upon PDA can be overcome by using the DPDA.

2 Experimental Set-up

The sending system shown in Figure 1 is identical with the systems used in standard PDA experiments, except that a high laser power

* Dipl.-Ing. J. Rheims, Prof. Dr.-Ing. K. Bauckhage, Universität Bremen, Verfahrenstechnik, Postfach 330 440, 28359 Bremen (Germany).

** Dr.-Ing. T. Wriedt, Institut für Werkstofftechnik, Badgasteiner Str. 3, 28334 Bremen (Germany).

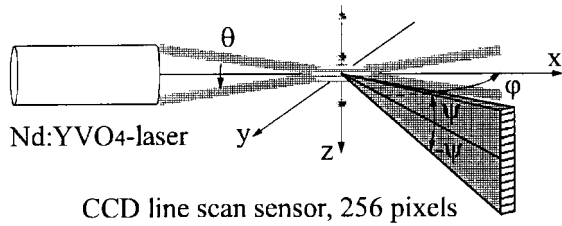


Fig. 1: Optical geometry of the differential PDA (DPDA).

of up to 3.5 W is needed owing to the smaller detector units. For this reason, a frequency-doubled Nd:YVO₄ laser emitting green light at $\lambda = 532$ nm is used [6]. The receiving system consists of a CCD line scan sensor with 256 pixels [7], arranged perpendicularly and symmetrically to the x,y-plane. The entire experimental set-up of the DPDA has been described elsewhere [8]. Arranging the sensor in the x,y-plane changes the composition of the detected signals and requires a different approach to signal analysis; this method, differential laser-Doppler anemometry or DLDA, is described elsewhere [8, 9].

The CCD sensor constantly transmits data to the digitization unit with a maximum line frequency of 98 kHz. The data are digitized to 8 bits corresponding to 256 gray levels and then transmitted to a PC. If the gray levels are beyond a threshold value, this is interpreted as burst signal which is evaluated as described in Section 4.

3 Optimization Procedure

As DPDA makes use of most of the optical principles of PDA, it is subject to the same scattering effects and the experimental set-up can be optimized by a similar procedure. For PDA this procedure is described, for instance, in Reference [10] and for DPDA in Reference [8]. In the following, the optimization procedure is outlined for water spheres in the size range 1–150 μm . Calculations are based on Mie theory and were performed with the PC-program *Scatap* [11].

For the sake of brevity, the following assumptions shall be introduced. The laser beams are polarized in the x,y-plane (parallel polarization). The half-beam crossing angle is $\theta/2 = 0.3^\circ$ and the resulting interference fringe spacing Δx is 51 μm . The line scan sensor covers an elevation angle range ψ from -12.5° to 12.5° . The off-axis angle ϕ is varied in the forward scattering direction because in this range, maximum intensity of scattered light is obtained. At 532 nm, water has the refractive index $n = 1.33 - i0.0$. It is transparent so that the scattered light contains different orders of refracted light in addition to the dominating first order. The experimental set-up, especially the position of the CCD line scan sensor, has to be optimized with respect to these particle characteristics.

Figure 2 shows the phase difference $\Delta\phi$ computed at $\phi = 38^\circ$ as a function of the elevation angle ψ , left baseline, and the particle diameter d , right baseline. $\Delta\phi$ is negative, and by definition this means that the scattering process is dominated by refracted light. Following those lines which are parallel to the right baseline, the phase difference-particle diameter relationship can be observed for a given elevation angle ψ . Figure 3 shows an example for an elevation angle $\psi = \pm 10^\circ$. This relationship is identical with that used in PDA to measure particle size, except that the small detection area of the CCD pixels causes strong oscillations in the function $\Delta\phi(d)$. Following the other baseline, the course of $\Delta\phi$ depending on the elevation angle ψ can be traced for a certain

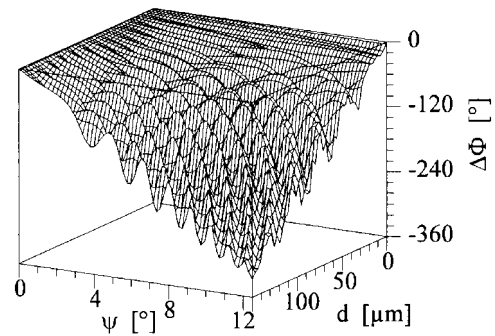


Fig. 2: Phase difference $\Delta\phi$ as function of particle diameter d and elevation angle ψ , calculated for parallel polarization and off-axis angle $\phi = 38^\circ$.

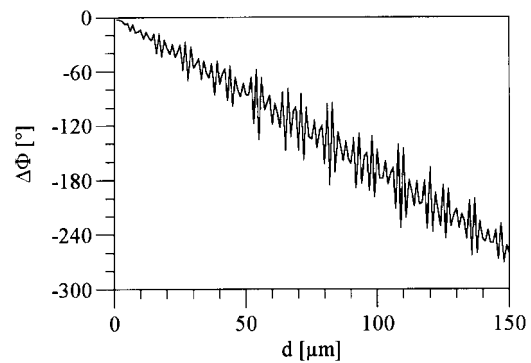


Fig. 3: Phase difference $\Delta\phi$ as function of particle diameter d , calculated for the elevation angle $\psi = 10^\circ$, parallel polarization and off-axis angle $\phi = 38^\circ$.

particle size. In Figure 4, the DPDA signal is depicted for a particle diameter of 50 μm . The entire function of $\Delta\phi(\psi, d)$, Figure 2, shows strong oscillations caused by the interference of the dominating first-order refracted light with higher orders of refraction and with light reflected at the particle surface. Therefore, the off-axis position $\phi = 38^\circ$ does not seem to be very suitable for DPDA measurements.

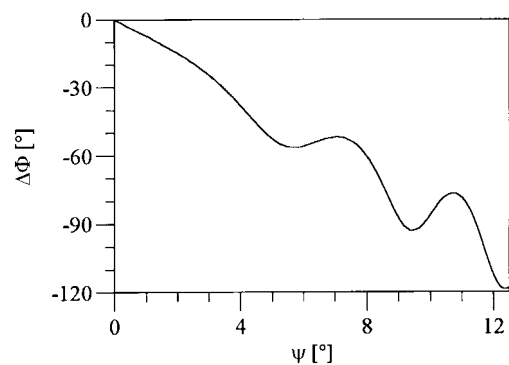


Fig. 4: Phase difference $\Delta\phi$ as function of elevation angle ψ , calculated for the particle diameter $d = 50 \mu\text{m}$, parallel polarization and off-axis angle $\phi = 38^\circ$.

By changing ϕ to 52° , these oscillations are reduced significantly, as shown in Figure 5. This is due to the well-known fact that for parallel polarized light and for an off-axis angle range ϕ between approximately 20° and 70° , the intensity ratio of refracted to reflected light increases with increase in ϕ . The disadvantage of this set-up is the lower intensity of scattered light, by about one

order of magnitude. The improved signal quality can also be seen in Figures 6 and 7, which show the dependence of $\Delta\phi$ on the particle diameter (Figure 6) and on the elevation angle ψ (Figure 7).

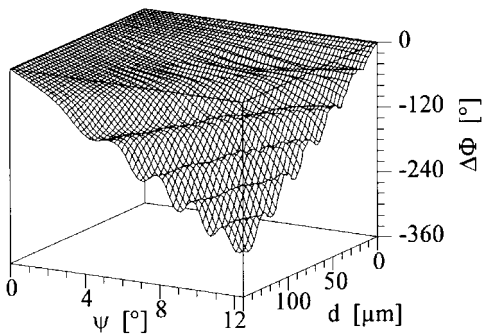


Fig. 5: Phase difference $\Delta\phi$ as function of particle diameter d and elevation angle ψ , calculated for parallel polarization and off-axis angle $\varphi = 52^\circ$.

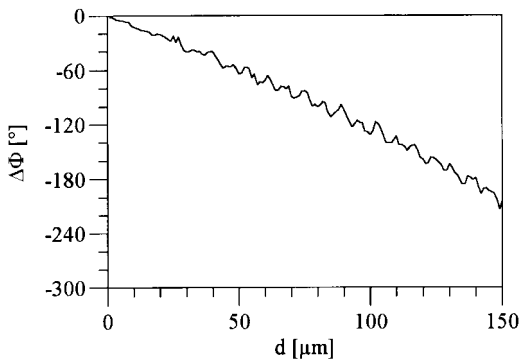


Fig. 6: Phase difference $\Delta\phi$ as function of particle diameter d , calculated for the elevation angle $\psi = 10^\circ$, parallel polarization and off-axis angle $\varphi = 52^\circ$.

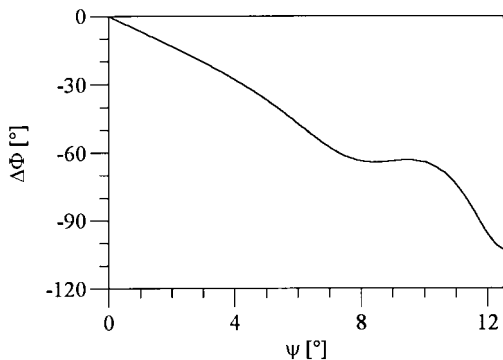


Fig. 7: Phase difference $\Delta\phi$ as function of elevation angle ψ , calculated for the particle diameter $d = 50 \mu\text{m}$, parallel polarization and off-axis angle $\varphi = 52^\circ$.

To evaluate the DPDA signals, linear regression analysis is applied to the function $\Delta\phi(\psi)$. $\Delta\phi$ is zero at $\psi = 0^\circ$ so that the only remaining unknown is the slope of the regression line. This parameter, γ , is defined by

$$\gamma = \frac{\overline{\Delta\phi}}{\overline{\psi}}. \quad (1)$$

Figure 8 shows this parameter as function of the particle diameter d . It can be seen that a higher off-axis angle is the preferred set-up for DPDA measurements, because the oscillations in the course of γ versus d decrease with increasing φ .

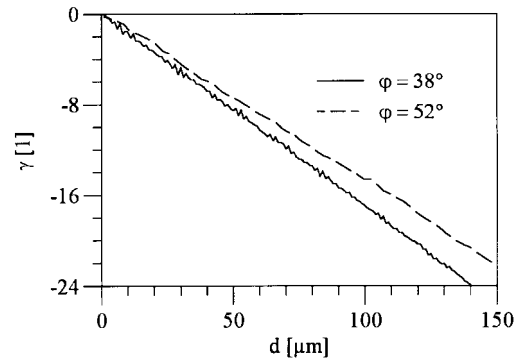


Fig. 8: Gradient γ versus particle diameter d ; γ was calculated from linear regression analysis of $\Delta\phi = f(\psi)$.

4 Signal Evaluation

The signal evaluation scheme used in DPDA can be explained by the use of Figure 9. In the first step, the time-resolved signal (top) of every pixel is subjected to a fast Fourier transform (FFT) [12]. This reveals the time-resolved frequency pattern of the burst at each pixel position respectively elevation angle, separated into the magnitude and phase of each frequency.

The magnitudes of the 256 frequency spectra are shown in the middle section of Figure 9. Each spectrum is analyzed with respect to the spectral line of highest magnitude, i.e. the dominant frequency. The course of the dominant frequency, obtained in this manner versus the elevation angle ψ , is also included in the middle part of Figure 9.

In the next step, averaging is applied to these data, followed by interpolation. In the case of the example data set, this leads to a medium dominant spectral line of 20.2. With knowledge of

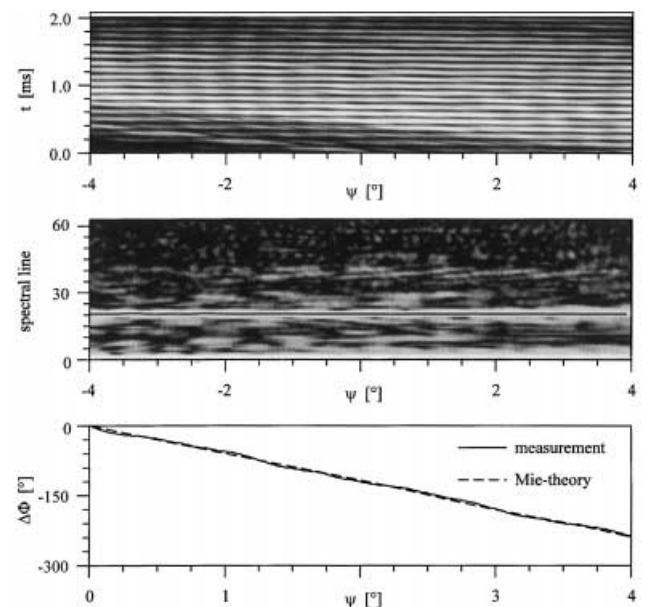


Fig. 9: Glass sphere 1 with intact surface: DPDA-burst (top), magnitude of FFT spectrum (middle) and phase difference in comparison with Mie theory (bottom).

the interference fringe spacing Δx , $51 \mu\text{m}$, and the line scan frequency of the sensor, 50.4 kHz , a particle velocity of 0.40 m/s is calculated.

To obtain particle size, the phase is determined at the average dominant spectral line of each pixel. Thereafter, a phase difference $\Delta\phi$ is calculated where the detector pairs are arranged symmetrically to the x,y -plane, which is the plane of symmetry of the entire set-up. The phase difference $\Delta\phi$ as a function of the elevation angle ψ is shown in the bottom section of Figure 9. Regression analysis is applied to this data set; the measured gradient γ is calculated according to Eq. (1), the result being $\gamma = -59.1$. Finally, with the function $d = f(\gamma)$ known from theoretical analysis, this yields the particle diameter, in the present case $d = 517 \mu\text{m}$.

5 Experimental Results

5.1 Glass Beads

To verify the DPDA, transparent glass spheres (Schott, type LaSf 35, $n_{532 \text{ nm}} = 2.04$ [13]) were attached to thin wires ($100 \mu\text{m}$ diameter), mounted on the shaft of a rotating electric motor and thus moved through the measuring volume repeatedly. The particle reference diameter was determined under a microscope and the reference velocity was calculated from the speed of the motor and the circumference of the particle trajectory. This led to reference data with which the PDA and DPDA measurements could be compared. The correlation between the measured gradient γ and the particle diameter was calculated as

$$\frac{d}{\mu\text{m}} = -8.74\gamma + 0.85. \quad (2)$$

The CCD sensor was arranged under an off-axis angle $\varphi = 52^\circ$ and covered an elevation angle range ψ from -4° to 4° ; the range observed by each pixel was $d = d\psi = 0.03^\circ$. For comparison, additional measurements were performed with a standard PDA system. The PDA detectors were also set to $\varphi = 52^\circ$, but with an elevation angle ψ of $\pm 3.1^\circ$. The angles covered by the rectangular PDA apertures were $d = 9.2^\circ$ and $d\psi = 1.2^\circ$. In both cases, the sending system was arranged as described in Section 3. The interference volume had a diameter d_z of 2.2 mm .

Prior to the complete experimental results, two selected single results will be considered. They were obtained with two glass spheres of different surface shapes. Figure 10 shows on the left a photograph of glass sphere 1 with apparently intact surface, and on the right particle 2 with poor surface quality. The DPDA burst of particle 1 (Figure 9, top) shows a distinct temporal modulation of the signal burst. Furthermore, the temporal shift of the signal with pixel position can be seen. As expected, the scattered light is first detected by the uppermost pixel. The frequency spectrum

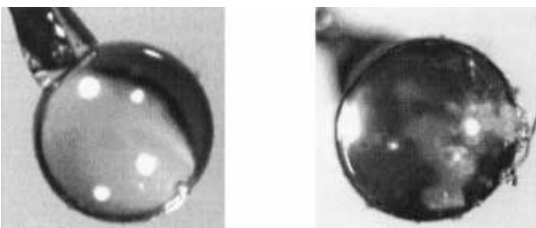


Fig. 10: Photographs of the two glass beads investigated: glass sphere 1 with intact surface (left), glass sphere 2 with defect surface (right).

(Figure 9, middle) obtained by a FFT in the temporal direction also shows very sharp dominant spectral lines. The following evaluation gives an average spectral line of 20.2 which transforms to a particle velocity of 0.40 m/s , in comparison with a reference velocity of 0.41 m/s . The phase difference calculated at this spectral line (Figure 9, bottom) results in a gradient $\gamma = -59.1$, and the particle size calculated from this value is $517 \mu\text{m}$, as is the reference diameter.

The DPDA signal of particle 2 (Figure 11) shows a much less clearly modulated signal. These distortions propagate into the FFT spectrum and into the relation between the phase difference $\Delta\phi$ and the elevation angle ψ . The measured particle velocity and size ($v = 0.46 \text{ m/s}$, $d = 512 \mu\text{m}$) are still close to reference data ($v = 0.45 \text{ m/s}$, $d = 500 \mu\text{m}$).

Tables 1 and 2 show, together with reference data, the results of 400 DPDA and PDA signals obtained from repeated measurements on the same particle. The standard deviation given for the reference data is an estimate of random and systematic errors in the calibration process; in the case of PDA and DPDA, the standard

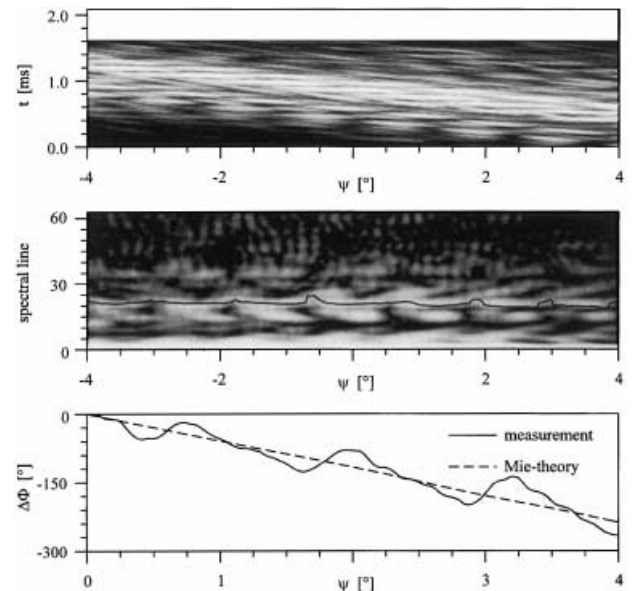


Fig. 11: Glass sphere 2 with surface defects: DPDA burst (top), magnitude of FFT spectrum (middle) and phase difference in comparison with Mie theory (bottom).

Table 1: Diameters of two glass beads measured with DPDA and PDA. Mean values and standard deviations of DPDA and PDA were calculated from 400 measurements on the same particle.

Bead	DPDA $d [\mu\text{m}]$	PDA $d [\mu\text{m}]$	Reference $d [\mu\text{m}]$
1	512.5 ± 4.6	483.2 ± 20.3	517 ± 3
2	505.3 ± 21.9	435.4 ± 23.0	500 ± 3

Table 2: Velocities of two glass beads measured with DPDA and PDA. Mean values and standard deviations of DPDA and PDA were calculated from 400 measurements on the same particle.

Bead	DPDA $v [\text{m/s}]$	PDA $v [\text{m/s}]$	Reference $v [\text{m/s}]$
1	0.40 ± 0.00	0.40 ± 0.01	0.41 ± 0.03
2	0.46 ± 0.00	0.45 ± 0.01	0.45 ± 0.03

deviation is only attributed to random errors occurring in the course of measurements. In the case of DPDA, very good coincidence with reference data and a very low standard deviation are obtained for both particle size and velocity. In the case of PDA, only the velocity is determined correctly, but the measured particle diameters differ significantly from the reference values. This implies that the characteristic spectral line is determined correctly but owing to the aforementioned defects on the particle surface and within the particle, the phase information is corrupted.

5.2 Small Water Droplets

In the next step, monodisperse water droplets generated by a piezoelectric droplet generator [14] were investigated. The diameter d_z of the interference volume was reduced to $550\ \mu\text{m}$ and the interference fringe spacing was $\Delta x = 51\ \mu\text{m}$. The CCD sensor was operated at the maximum frequency of $98\ \text{kHz}$ and detected the scattered light between $-12.5^\circ \leq \psi \leq 12.5^\circ$ at a range of $d\varphi = d = 0.1^\circ$ per pixel. For comparison, two DPDA measurements were performed at $\varphi = 38^\circ$ and at $\varphi = 52^\circ$. The PDA detectors were arranged at $\varphi = 52^\circ$ and $\psi = \pm 3.1^\circ$ and covered the same angle range as before: $d\varphi = 9.2^\circ$, $d\psi = 1.2^\circ$.

Table 3 shows the mean values of the measured particle sizes and their standard deviations, calculated for 400 PDA and DPDA signals. The results demonstrate that the DPDA can be applied to particles with a minimum diameter of $25\ \mu\text{m}$. Comparing the DPDA results measured at $\varphi = 38^\circ$ and at $\varphi = 52^\circ$, it can be seen that the lower off-axis angle gives better results. The reverse effect was expected from theoretical investigations, but the reason is that the intensity of scattered light is approximately one order of magnitude lower at $\varphi = 52^\circ$. Therefore, noise plays a more important role and seems to corrupt the scattered light. This adversely affects the accuracy of measurements, i.e. the standard deviation increases, and makes measurements impossible at $\varphi = 52^\circ$ for droplets with a diameter of $25\ \mu\text{m}$ or less. Comparing the DPDA and PDA results, no significant difference can be seen. The reason is that the surface tension forces the liquid droplets into a perfect spherical shape without any surface defects so that ideal experimental conditions exist.

Table 3: Diameters of three types of monodisperse water sprays measured with DPDA and PDA. Mean values and standard deviations of DPDA and PDA were calculated from 400 measurements.

Spray	DPDA, $\varphi = 38^\circ$ $d\ [\mu\text{m}]$	DPDA, $\varphi = 52^\circ$ $d\ [\mu\text{m}]$	PDA, $\varphi = 52^\circ$ $d\ [\mu\text{m}]$	Reference $d\ [\mu\text{m}]$
1	25.3 ± 0.5	no result	25.0 ± 0.7	25 ± 3
2	49.6 ± 1.9	48.2 ± 3.5	49.6 ± 2.4	50 ± 3
3	73.1 ± 6.1	69.4 ± 5.4	72.5 ± 3.8	75 ± 3

6 Conclusions

The theoretical and experimental results presented in this paper demonstrate the possibilities of a new method for measuring particle size and velocity, differential PDA. Compared with standard PDA, DPDA has the potential for exact size determination

even under severe conditions such as glass spheres with surface defects or inhomogeneous composition. If better experimental conditions with respect to particle surface and composition exist, no difference can be seen between PDA and DPDA. The smallest particles measured with DPDA so far, water droplets, have a diameter of $25\ \mu\text{m}$. Size measurements down to $10\ \mu\text{m}$ seem to be possible.

7 Acknowledgements

We acknowledge the support by the DFG (Deutsche Forschungsgemeinschaft) under grant Wr 22/4-2.

8 Symbols and Abbreviations

d	particle diameter [mm]
d_z	diameter of the measuring volume in the direction of z [μm]
n	complex refractive index [1]
n'	real part of the complex refractive index n [1]
t	time [s]
γ	slope of the regression line in DPDA signal analysis [1]
Δx	interference fringe spacing [μm]
$\theta/2$	half-beam crossing angle [$^\circ$]
κ	absorption index, imaginary part of the complex refractive index n [1]
λ	laser light wavelength [nm]
$\Delta\phi$	phase difference between Doppler bursts [$^\circ$]
$\bar{\Delta\phi}$	mean value of the phase difference $\Delta\phi$ [$^\circ$]
φ	off-axis angle [$^\circ$]
$d\varphi$	aperture size in direction of φ [$^\circ$]
ψ	elevation angle [$^\circ$]
$\bar{\psi}$	mean value of the elevation angle ψ [$^\circ$]
$d\psi$	aperture size in direction of ψ [$^\circ$]

9 References

- [1] *E. D. Hirleman*: History of development of the Phase-Doppler Particle-Sizing Velocimeter. Part. Part. Syst. Charact. 13 (1996) 59–67.
- [2] *K. Bauckhage*: Gleichzeitige Erfassung von Partikelmerkmalen und Eigenschaften mehrphasiger Strömungen mit Hilfe der Phasen-Doppler-Anemometrie. Chem.-Ing.-Tech. 68 (1996) 253–266.
- [3] *C. Tropea, T. H. Xu, F. Onofri, G. Gréhan, P. Haugen, M. Stieglmeier*: Dual-Mode Phase-Doppler Anemometer. Part. Part. Syst. Charact. 13 (1996) 165–170.
- [4] *O. Köser, T. Wriedt*: Iterative Inversion of Phase-Doppler-Anemometry Size Distributions from Sprays of Optically Inhomogeneous Liquids. Appl. Opt. 35 (1996) 2537–2543.
- [5] *M. Mitschke, T. Wriedt, K. Bauckhage*: Standard PDA for Measuring the Size of Inhomogeneous Droplets. Meas. Sci. Technol. 9 (1998) 193–205.
- [6] *Spectra Physics Lasers*: Millennia, Diode-pumped, Nd:YVO₄ CW Laser: User's Manual. Mountain View, USA 1996.
- [7] *Dalsa Inc.*: Cl-Cx Camera User's Manual. Waterloo, Canada 1994.
- [8] *J. Rheims*: Partikelanalyse mittels differentieller Streulichtmessungen unter hoher räumlicher und zeitlicher Auflösung. Fortschr. Ber. VDI, Reihe 8, Nr. 710, Düsseldorf, VDI-Verlag, 1998.

- [9] *J. Rheims, T. Wriedt, K. Bauckhage*: Sizing of Inhomogeneous Particles by a Differential Laser Doppler Anemometer. Submitted to Meas. Sci. Technol.
- [10] *Dantec Measurement Technology*: PDA User's Manual. Skovlunde, Denmark 1992.
- [11] *Scatap* is available at <http://imperator.cip=iw1.uni-bremen.de/fg01/scatap.html>.
- [12] *T. Wriedt, K. Bauckhage, A. Schöne*: Application of Fourier Analysis to Phase-Doppler-Signals generated by Rough Metal particles. IEEE Trans. Instrum. Meas. IM-38 (1989) 5, 984–990.
- [13] *Schott Glaswerke*: Optisches Glas Nr. 10000 D. Mainz, Germany 1996.
- [14] *H. Ulmke, T. Wriedt*: Piezoelektrischer Tropfengenerator zur Kalibrierung von Partikelzählern. Unpublished work.